Calculation of wakefields in a 17 GHz beam-driven photonic band-gap accelerator structure

Min Hu*

Terahertz Research Center, School of Physical Electronics,
University of Electronic Science and Technology of China, Chengdu 610054, China,
and Plasma Science and Fusion Center, Massachusetts Institute of Technology, Cambridge, Massachusetts 02139, USA

Brian J. Munroe, Michael A. Shapiro, and Richard J. Temkin

Plasma Science and Fusion Center, Massachusetts Institute of Technology, Cambridge, Massachusetts 02139, USA
(Received 30 August 2012; published 11 February 2013)

We present the theoretical analysis and computer simulation of the wakefields in a 17 GHz photonic band-gap (PBG) structure for accelerator applications. Using the commercial code CST PARTICLE STUDIO, the fundamental accelerating mode and dipole modes are excited by passing an 18 MeV electron beam through a seven-cell traveling-wave PBG structure. The characteristics of the longitudinal and transverse wakefields, wake potential spectrum, dipole mode distribution, and their quality factors are calculated and analyzed theoretically. Unlike in conventional disk-loaded waveguide (DLW) structures, three dipole modes (TM_{11}-like, TM_{12}-like, and TM_{13}-like) are excited in the PBG structure with comparable initial amplitudes. These modes are separated by less than 4 GHz in frequency and are damped quickly due to low radiative Q factors. Simulations verify that a PBG structure provides wakefield damping relative to a DLW structure. Simulations were done with both single-bunch excitation to determine the frequency spectrum of the wakefields and multibunch excitation to compare to wakefield measurements taken at MIT using a 17 GHz bunch train. These simulation results will guide the design of next-generation high-gradient accelerator PBG structures.

DOI: 10.1103/PhysRevSTAB.16.022002 PACS numbers: 29.20.Ej

I. INTRODUCTION

Future high-energy accelerators will require high-gradient electromagnetic fields to accelerate the electron beam to obtain high luminosity. Besides the accelerating mode, high order modes (HOMs) are excited in the accelerator cavity which will affect the electron beam and decrease the accelerating efficiency and beam stability. The electromagnetic fields generated in the accelerator structure by passing charged particles are called wakefields. Wakefield damping is an important consideration for the design of future high-gradient accelerator structures. Many innovative methods have been proposed to provide sufficient wakefield damping for high-energy accelerators. These methods include HOM damping couplers [1], choke-mode structures [2,3], damped, detuned structures (DDS) [4,5], Compact Linear Collider structure with waveguide HOM damping [6], square [7] and triangular lattice metallic photonic band-gap (PBG) structures [8,9], and dielectric PBG structures [10–13].

The goal of PBG accelerator structures is to provide a structure with very high wakefield damping across all HOM frequencies. To validate this design goal, and to design the next set of experimental PBG structures, the wakefields in a PBG structure need to be calculated and compared to the wakefields in other types of accelerator structures. This will allow the development of a theory by which to predict the wakefields in new PBG designs, and provide a quantitative evaluation of the damping in the PBG structure.

The general theoretical work for the analytical calculation of wakefields has been developed in [14–17]. The wake potential is the summation over all the structure modes excited by the impulse. The longitudinal and transverse wake potentials in cylindrically symmetric structures can be written as [14,17]

$$\begin{aligned} W_z(r',r,s) &= \sum_{m=0,n=1}^{\infty} 2\left(\frac{r'}{d}\right)^m \left(\frac{r}{d}\right)^m \cos(m\theta) k_{zmn}(d) \\ &\quad \times \cos\left(\frac{\omega_{mn} s}{c}\right) \exp\left(-\frac{\omega_{mn} s}{2Q_{mn} c}\right), \\ \boldsymbol{W}_\perp(r',r,s) &= \sum_{m,n=1}^{\infty} 2m\left(\frac{r'}{d}\right)^m \left(\frac{r}{d}\right)^{m-1} [\hat{r}\cos(m\theta) \\ &\quad - \hat{\theta}\sin(m\theta)] k_{\perp mn}(d) \sin\left(\frac{\omega_{mn} s}{c}\right) \\ &\quad \times \exp\left(-\frac{\omega_{mn} s}{2Q_{mn} c}\right), \end{aligned} \tag{1}$$

where s is the distance behind the driving bunch, r' is the displacement of the driving bunch, r is the test beam

*hu_m@uestc.edu.cn

transverse position, d is the radius of the iris aperture, k_{zmn} is the loss factor, $k_{\perp mn}$ is the kick factor, ω_{mn} is the frequency, c is the speed of light, and Q_{mn} is the quality factor of the TM_{mn} mode. In Eq. (1),

$$k_{zmn}(d) = \frac{|V_{mn}(d)|^2}{4U_{mn}}, \tag{2}$$

$$k_{\perp mn}(d) = \frac{k_{zmn}(d)}{\omega_{mn} d/c}, \tag{3}$$

where V_{mn} is the voltage along one period and U_{mn} is the stored energy in the TM_{mn} mode. From Eq. (1) we can see that the initial transverse wake potential depends on the kick factor $k_{\perp mn}$, and damping is induced by the damping factor $\exp(-\omega_{mn} s/2Q_{mn}c)$. Low initial transverse wake potential can be reached by decreasing the kick factors of the modes, but effective wake potential damping can be achieved primarily by decreasing the quality factor Q_{mn}.

The longitudinal and transverse wake potentials are described in the time domain. We define corresponding longitudinal and transverse impedances for the frequency-domain description [16]:

$$\begin{aligned} Z_z(\omega) &= \frac{1}{c}\int_{-\infty}^{\infty} W_z(s) e^{-j\omega s/c} ds, \\ Z_\perp(\omega) &= \frac{1}{jc}\int_{-\infty}^{\infty} W_\perp(s) e^{-j\omega s/c} ds. \end{aligned} \tag{4}$$

The above formulas can be used to analytically calculate the wake potentials in right-cylinder structures in which the electromagnetic fields can be expressed in a closed form, such as pillbox resonators [18] and disk-loaded waveguide structures [19,20] with excitation by a point charge [21] or charged rings [22].

The frequency selectivity of photonic band-gap (PBG) structures makes them appealing for wakefield damping in accelerator applications. By introducing a defect in the center of a triangular lattice of metallic rods, a PBG cavity can be formed which confines a particular operating mode and lets other modes radiate through the lattice. This radiative damping decreases the Q factor of the dipole modes, making the wake damp faster. This kind of PBG structure has been extensively researched theoretically and experimentally [23–25]. A 17 GHz six-cell traveling-wave PBG accelerator structure has previously been designed, simulated, and tested at the MIT Plasma Science and Fusion Center (PSFC) [8,9].

Previous theoretical work suggested that HOMs are not supported in PBG structures [8]. Later theoretical and experimental research indicated that HOMs do exist in PBG structures, but with low Q and high loss [9].

Previous experimental work has shown that PBG structures composed entirely of round rods can operate at gradients above 80 MV/m [26]. This performance can be improved by giving the rods closest to the defect region elliptical cross sections, while keeping the other rods round. A PBG structure with this rod configuration has been shown to operate at a gradient above 125 MV/m [27]. This work represents the first step in the analysis of the wakefield damping in these high-gradient PBG structures, which in turn will guide the design of future high-gradient PBG structures for testing with and without beam.

In this paper, we report the results of PIC simulations of the wake potential in a seven-cell 17 GHz PBG structure based on the structure tested at MIT. Both six- and seven-cell structures were simulated, with the seven-cell simulation showing more initial promise. While the results presented here are for the seven-cell structure, all the wakefield results have been reproduced using a six-cell model. In both cases the model is simplified from the structure tested at MIT; the CST models all have uniform cells while the MIT experimental structure has coupling cells and waveguides forming the first and sixth cells.

The results from CST PARTICLE STUDIO show that there are three dipolelike modes: TM_{11}-like, TM_{12}-like, and TM_{13}-like, which are excited by an off-axis electron beam. In this paper, the notation of TM_{mn} means that the mode has m azimuthal variations and n radial variations in the entire PBG cross section, not just in the defect area. The total wake potential and the characteristics of each dipole mode are analyzed. An equivalent disk-loaded waveguide structure is also simulated and the wakefields are compared to the PBG structure, showing that the PBG structure damps the transverse wakefield effectively. The structure of this paper is: the wake potential and spectrum calculation is in Sec. II, the analysis of the dipole modes is shown in Secs. III and IV demonstrates the comparison results between PBG and disk-loaded waveguide (DLW) structures, multibunch simulation and beam loading calculation are described in Sec. V, and finally the paper is concluded in Sec. VI.

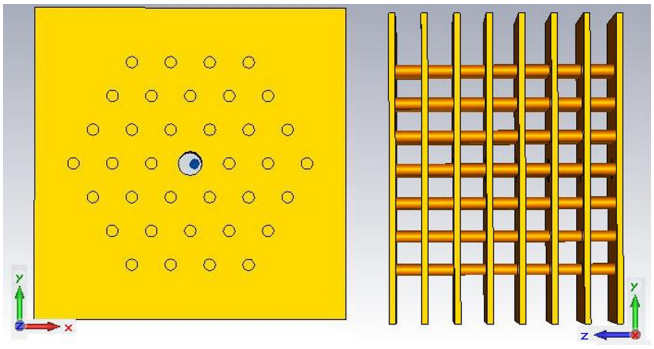

FIG. 1. Schematic of a seven-cell PBG structure. The structure is formed by three rows of a triangular lattice of metallic cylindrical rods. The central rod is removed to form a defect region to confine the fundamental TM_{01} mode. The dimensions are given in Table I.

TABLE I. Dimensions of the PBG structure.

Geometric parameters	Value
Rod radius, a	1.04 mm
Rod spacing, b	6.97 mm
Iris thickness, t	1.14 mm
Iris radius, d	2.16 mm
Cavity length, L	5.83 mm
TM_{01} mode frequency	17.14 GHz
Accelerating mode	$2\pi/3$ mode
Number of cells	7

II. WAKE POTENTIAL CALCULATION

The PBG structure with three rows of metallic rods is shown in Fig. 1 and the dimensions of the PBG structure are shown in Table I. All the parameters of this 17 GHz PBG structure come from the traveling-wave PBG structure design [8] which has been tested at MIT [9]. Wake potentials and wake potential impedances are calculated per meter of structure length. The wakefield module in CST PARTICLE STUDIO is used to calculate the longitudinal and transverse wake potentials. The simulations considered both the Ohmic loss due to the finite conductivity of the copper structure and diffractive losses due to power incident on the absorptive boundary layer surrounding the structure. In the experimental test of the structure, the diffracted power was dissipated by diffuse reflections in a large external vacuum chamber; dissipation of this power in an accelerator structure represents a future engineering challenge.

For single-bunch measurements, an electron beam of zero transverse dimension and a 1 mm Gaussian length is injected into the beam tunnel with a 0.8 mm displacement in the x direction, as shown in Fig. 1. We have also calculated the wake potentials with the same beam displacement in the y direction, and the results are the same.

The longitudinal and transverse wake potential are shown as a function of distance behind the bunch in Figs. 2(a) and 3(a). The longitudinal and transverse wake potential impedances are obtained to analyze frequency-domain features in Figs. 2(b) and 3(b).

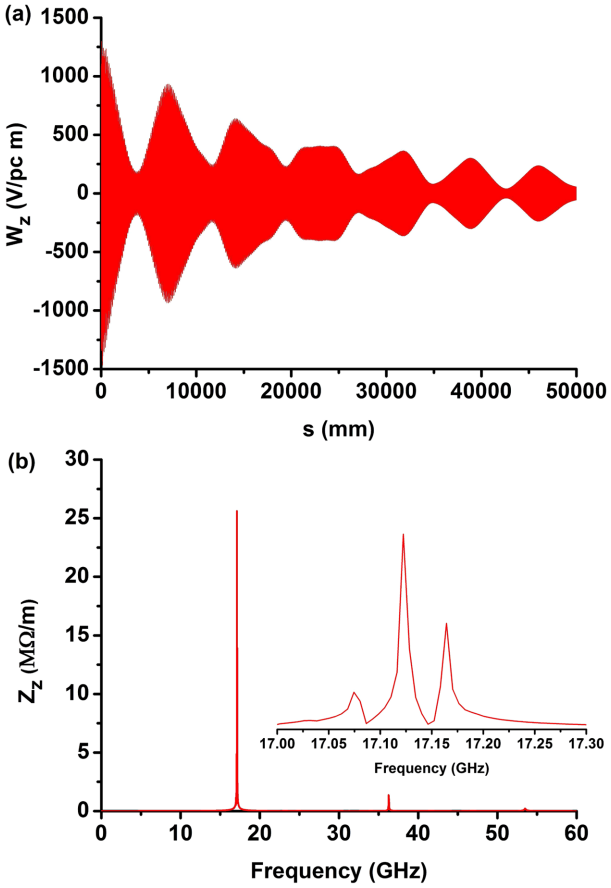

FIG. 2. Calculation of longitudinal wake potential and impedance: (a) longitudinal wake potential on a line parallel to the structure centerline and displaced 0.8 mm in the x direction, i.e., following the path of the beam; (b) longitudinal wake potential impedance.

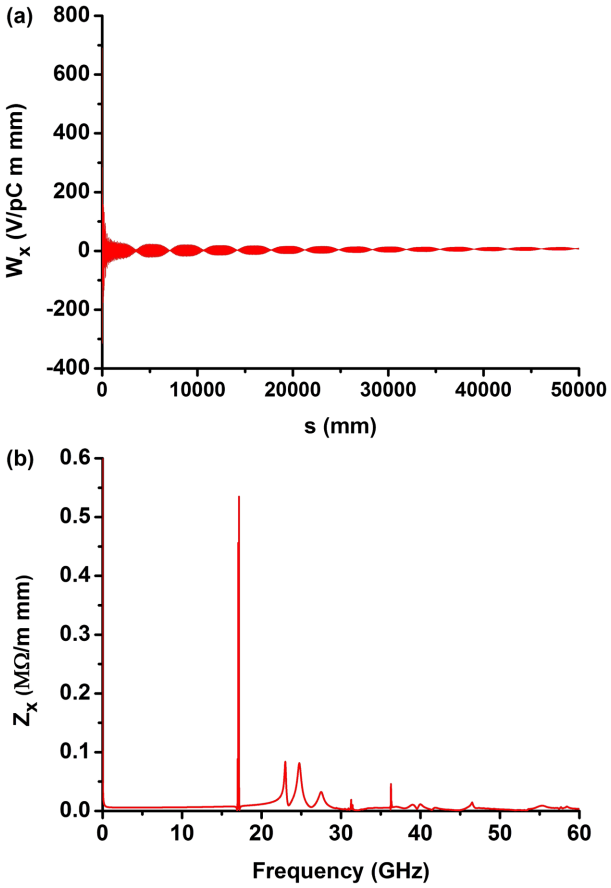

FIG. 3. Calculation of transverse wake potential and impedance: (a) transverse wake potential on a line parallel to the structure centerline and displaced 0.8 mm in the x direction, i.e., following the path of the beam; (b) transverse wake potential impedance.

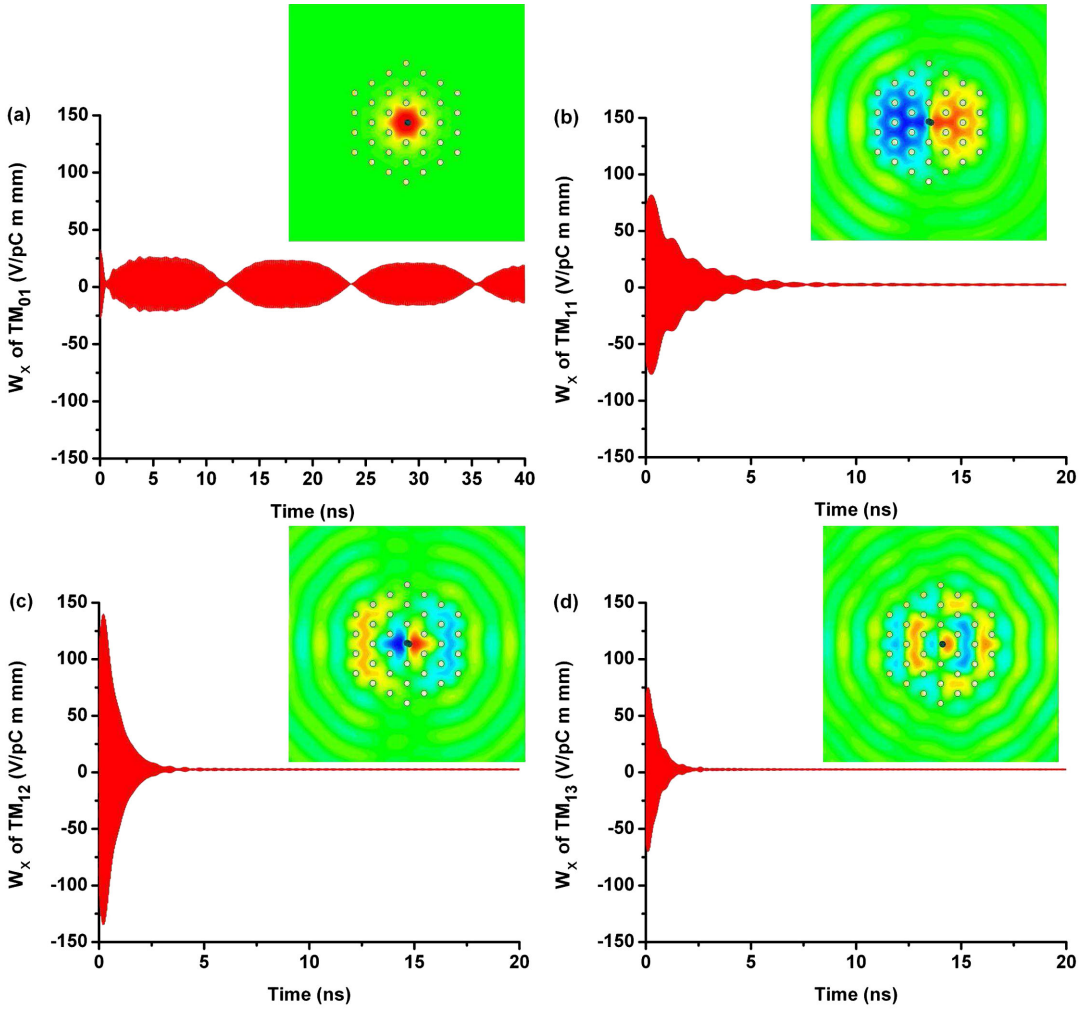

FIG. 4. Transverse wake potential as a function of time for each mode in the PBG structure: (a) TM_{01}-like mode at 17.1 GHz; (b) TM_{11}-like mode at 23.0 GHz; (c) TM_{12}-like mode at 24.8 GHz; (d) TM_{13}-like mode at 27.5 GHz.

The longitudinal wake potential calculated on the beam track decays slowly, as shown in Fig. 2(a). The normalized frequency spectrum of the longitudinal wake potential shows that the fundamental mode has three peaks at 17.002, 17.092, and 17.176 GHz, as shown in top right of Fig. 2(b). These peaks reveal the different phase advances $(0, \pi/3, 2\pi/3)$ of the fundamental mode excited by a single bunch in the seven-cell PBG structure which agree with the previous theoretical analysis and the cold test in [8,28]. The fundamental frequency resolution in the spectrum is 6 MHz which is limited by the finite simulation length. The dipole modes do not contribute to the longitudinal wake because the longitudinal electric fields of dipole modes are zero in the center, so there is no peak.

The transverse wake potential, shown in Fig. 3(a), can be seen to damp much faster than the longitudinal wake potential. The transverse wake potential damps quickly because its main contributions come from the dipole modes and the dipole modes have small Q factors. The fundamental mode present in the frequency spectrum of the transverse wake potential is formed due to the irises and confined in the defect area. The high Q factor of the TM_{01} mode keeps the transverse wake potential at a small but stable value even 50 000 mm behind the electron beam. Three dipole modes are excited at 23.0, 24.8, and 27.5 GHz with comparable initial amplitudes. The field distributions of these modes are shown in Fig. 4. These modes are distinguished as TM_{11}-like, TM_{12}-like, and TM_{13}-like modes separately and all of these modes are not confined within the defect region, but radiate away from the center to the outer boundary. The detailed analysis of the dipole modes will be given in Sec. III.

III. DIPOLE MODE ANALYSIS

Figure 3(a) shows that the transverse wake potential in the PBG structure is quickly damped. The transverse wake is dominated by three dipole modes, with similar initial

TABLE II. Comparison of $1/e$ distances calculated from HFSS and CST simulation results.

Mode	Frequency (GHz)	Q value	HFSS $1/e$ distance	CST $1/e$ distance
TM_{01}-like	17.1	3955	2.2×10^4 mm	3.0×10^4 mm
TM_{11}-like	23.2	71	290 mm	480 mm
TM_{12}-like	24.7	57	220 mm	210 mm
TM_{13}-like	27.0	45	170 mm	140 mm

amplitudes and with frequencies within 4 GHz of each other. This indicates that the previous approach of considering only the lowest-frequency dipole mode is insufficient for predicting the transverse wake potential.

To isolate the contribution to the wake potential from each dipole mode independently, numerical filters were used to separate the different modes within the wake potential. The filtering was done in MATLAB using the digital signal processing toolbox. For each frequency a bandpass filter was applied in frequency space. An inverse fast Fourier transform was then applied to the filtered spectra to obtain the time-domain signal showing the damping for each dipole mode.

Figure 4 shows the separate frequency components of the transverse wake potential versus time ($t = s/c$) and the field distribution at each dipole mode frequency. The fundamental mode [Fig. 4(a)] is confined in the defect region in a PBG cavity with a high Q factor, providing a small, slow-decaying transverse wake potential. The transverse electric field component of the TM_{01} mode is caused by the irises. The beating visible in the fundamental mode is caused by the different fundamental modes shown in Fig. 2(b).

The lowest-frequency TM_{11}-like dipole mode [Fig. 4(b)] decays more slowly than the two other dipole modes. The TM_{12}-like dipole mode [Fig. 4(c)] reaches a maximum amplitude a short time after the bunch passes and decays faster than the TM_{11}-like mode. The TM_{13}-like mode [Fig. 4(d)] has the highest frequency and is excited with less than half of the intensity of the previous dipole modes and decays faster than either of the lower-frequency dipole modes. The relative intensity of these dipole modes agrees well with the wake potential spectrum shown in Fig. 3(b).

From Eq. (1), the decay of the wake potential is related to the damping factor $\exp(-\omega_{mn} s/2Q_{mn} c)$. Because the frequencies of these dipole modes are close, the quality factor of each mode is the dominant contributor to the damping of each mode.

To calculate the quality factor of each mode, eigenmode simulations are run with the same simulation environment as in CST PARTICLE STUDIO, i.e., a lossy copper structure with an absorbing boundary layer located outside of the PBG lattice. Because CST MICROWAVE STUDIO does not support the use of absorptive boundary layers in eigenmode simulations, the Ansys code HFSS, which does support absorptive boundary layers in eigenmode simulations, is used instead. All three dipole modes are found to have a phase advance per cell of approximately π in the CST simulation, so the phase advance per cell is set to $2\pi/3$ for the fundamental mode and π for the dipole modes in the HFSS simulations.

The results of the eigenmode calculations in HFSS are shown in Table II. The quality factors in Table II contain both the Ohmic losses and diffractive losses in the structure. The frequencies of the modes in the HFSS simulations agree well with the frequencies observed in the CST simulations.

The HFSS results provide good qualitative agreement with the damping times of the respective dipole modes calculated in the CST simulation. The $1/e$ distance of the wake potential, $(2Q_{mn}c)/\omega_{mn}$ from Eq. (1), is calculated for each mode from the Q factor and ω obtained from HFSS. The $1/e$ distance is also calculated from the decay distance of the wakes observed in CST. These two values of $1/e$ distance are shown in columns 3 and 4 of Table II. The two different simulation techniques give reasonable agreement between the decay distances for each mode. This validates the use of simple single-cell eigenmode models to predict approximate decay distances for modes excited by the beam.

Unlike in conventional disk-loaded waveguide structures, the different dipole modes in the PBG structure are excited with small differences in frequency. In order to determine the relationship between the number of dipole modes excited and the number of rows of rods in the PBG structure, two-row and four-row PBG structures were modeled in addition to the three-row structure. All the other parameters of each structure were unchanged from the three-row PBG structure, with the only change being the number of rows of rods in the structures.

The transverse wake potential impedances defined by Eq. (4) of these structures are shown in Fig. 5, and dipole mode frequencies are listed in Table III. In the two-row PBG structure, however, there are only two dipole modes; the TM_{11}-like mode at 23.6 GHz and the TM_{12}-like mode at 26.6 GHz. The impedance of the TM_{11}-like mode is higher than that in the three-row PBG, but the impedance of the TM_{12}-like mode is much smaller. In the four-row PBG structure there are four dipole modes excited; the TM_{11}-like mode at 22.7 GHz, the TM_{12}-like mode at 23.9 GHz, the TM_{13}-like mode at 25.7 GHz, and the TM_{14}-like mode at 27.8 GHz. The highest-impedance

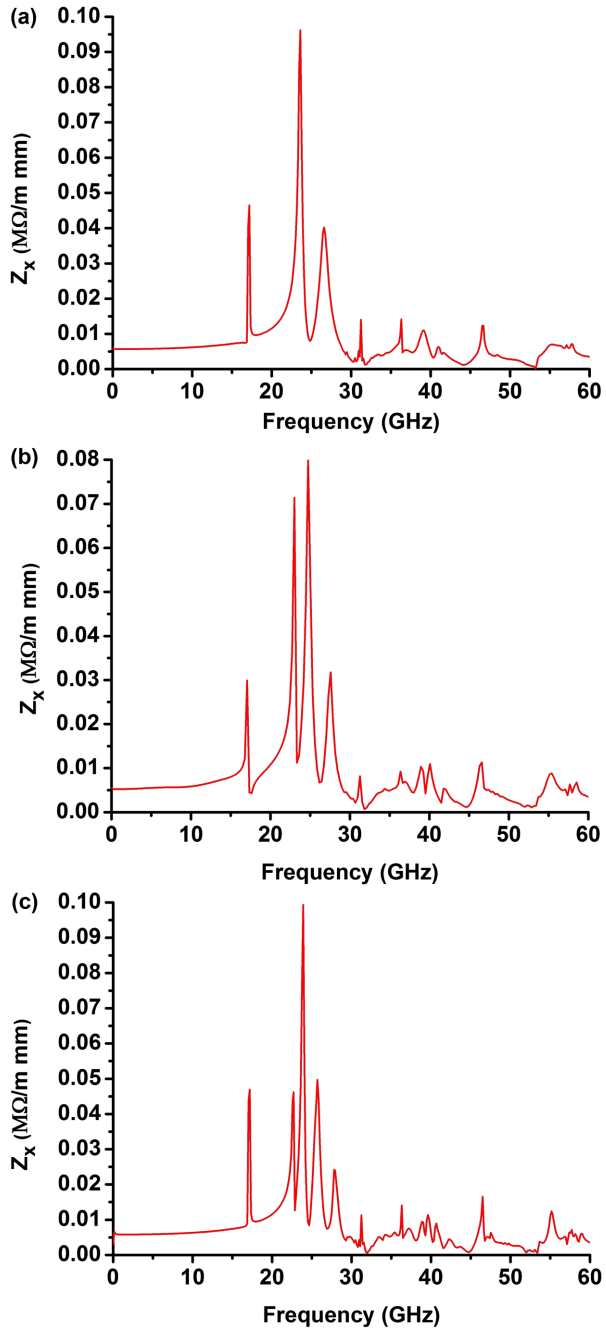

FIG. 5. Transverse wake potential impedances: (a) transverse wake potential impedance in a two-row PBG structure, two dipole mode peaks are at 23.6 and 26.6 GHz; (b) transverse wake potential impedance in a three-row PBG structure, three dipole mode peaks are at 23.0, 24.8, and 27.5 GHz; (c) transverse wake potential impedance in a four-row PBG structure, four dipole mode peaks are at 22.7, 23.9, 25.7, and 27.8 GHz.

dipole mode in the four-row PBG is the TM_{12}-like mode, as in the three-row PBG. The impedance of the TM_{14}-like mode is smaller by a factor of 4 than that of the highest-impedance dipole mode. From the above three situations, we can find that as the number of rows increases, more dipole modes are excited, but the frequencies of the dipole modes decrease. Unlike the DLW, the dipole modes of the PBG structure are spread out over a narrow frequency range. All modes listed in Table III are confirmed by the field distribution graphs in CST. Although the number of dipole modes are different and the dipole modes are at different frequency, the initial transverse wake potentials in the two-row, three-row, and four-row PBG structures are almost the same.

TABLE III. Dipole modes frequency of different row PBGs.

Dipole mode	Two-row PBG	Three-row PBG	Four-row PBG
TM_{11}-like	23.6 GHz	23.0 GHz	22.7 GHz
TM_{12}-like	26.6 GHz	24.8 GHz	23.9 GHz
TM_{13}-like		27.5 GHz	25.7 GHz
TM_{14}-like			27.8 GHz

IV. COMPARISON OF WAKE POTENTIAL IN PBG AND DLW

The previous results confirm that the PBG structure provides wake potential damping, although three dipole modes are excited. To compare the strength of the wake potential damping in the PBG structure we compare the wake potential between the PBG structure and an equivalent seven-cell traveling-wave disk-loaded waveguide structure with the same iris geometry, as shown in Table IV. We used the CST PS wakefield module to simulate the equivalent disk-loaded waveguide structure.

The transverse wake potentials for the disk-loaded waveguide structure and the PBG are shown in Fig. 6. From the theory, the quality factor of the PBG structure includes two parts: Q_{ohm} and Q_{diff}. Q_{ohm} depends on the Ohmic loss of copper, and Q_{diff} accounts for the diffractive loss in the structure. The Q_{diff} in the disk-loaded waveguide structure is very large because of the closed cavities, so the total Q in the disk-loaded waveguide structure depends only on the Ohmic Q. The diffractive Q of the fundamental mode in the PBG is finite but much larger than Q_{ohm} because this mode frequency lies in the band gap of the structure.

TABLE IV. Dimensions of the DLW structure.

Geometric parameters	Value
Cavity radius, b	6.91 mm
Iris thickness, t	1.14 mm
Iris radius, d	2.16 mm
Cavity length, L	5.83 mm
Accelerating mode	$2\pi/3$ mode
Number of cells	7

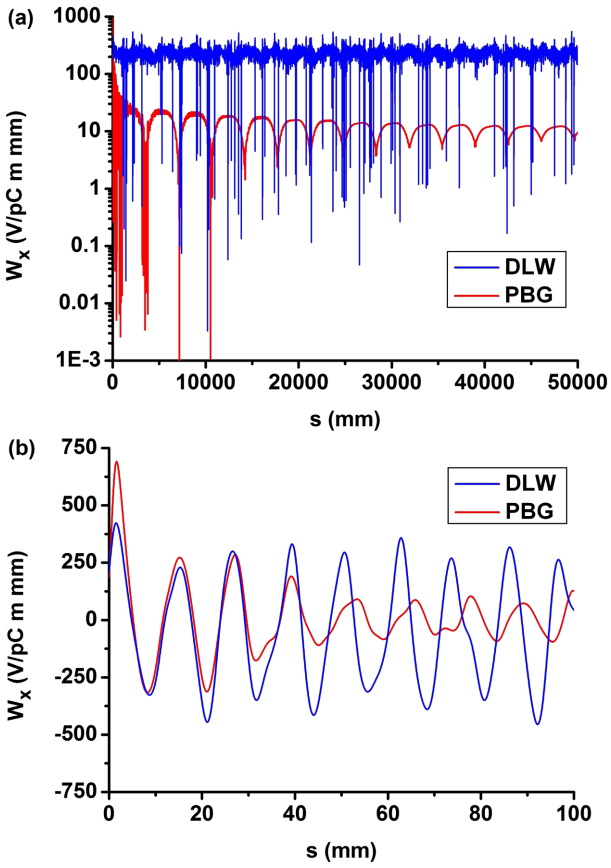

FIG. 6. Comparison of transverse wake potential between DLW and PBG structures. The blue line is DLW wake potential, and the red is PBG wake potential: (a) the envelope of transverse wake potential in DLW and PBG along 50 000 mm; (b) the first 100 mm transverse wake potential in both structures.

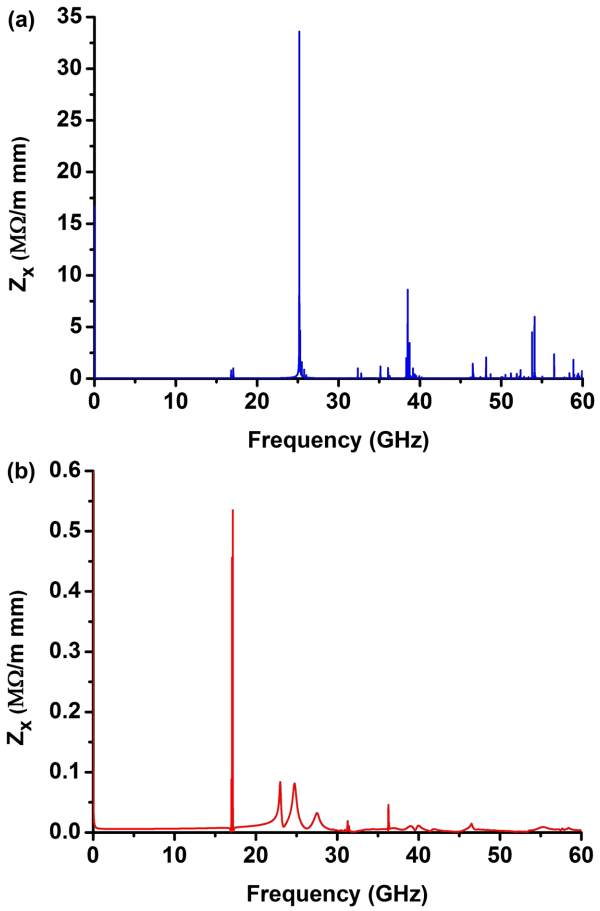

FIG. 7. Comparison of transverse wake potential impedances between PBG and DLW structures: (a) the transverse wake potential impedance in the DLW; (b) the transverse wake potential impedance in the PBG [same as Fig. 3(b)].

Figure 6 shows the comparison of the transverse wake potential between the disk-loaded waveguide structure and the PBG structure. This clearly indicates that the wake potential in the PBG structure damps much faster than in the disk-loaded waveguide structure. In the PBG structure the transverse wake potential is highly damped within the first 500 mm, whereas the transverse wake potential in the disk-loaded waveguide structure is not significantly damped even at 50 000 mm after the drive bunch. This proves that the PBG structure provides significant damping of the transverse wake potential relative to a disk-loaded waveguide structure. Figure 6(b) shows a detail of the first 100 mm of the transverse wake potential, indicating that the initial amplitude of the transverse wake potential in both structures is approximately the same, but the wake in the PBG structure shows significant damping after the first 30 mm.

Figure 7 shows the comparison of the transverse spectrum between the PBG and the disk-loaded waveguide structure. Figure 7(a) shows that in the disk-loaded waveguide structure the TM_{11} π mode (25.1 GHz) has an extremely high peak, and the next higher peaks appear at 38.5 GHz and 54.5 GHz. In conclusion, all of these simulations demonstrate the effective damping of wakefields in PBG structures designed for accelerator applications.

V. MULTIBUNCH SIMULATION AND BEAM LOADING CALCULATION

A six-cell PBG structure with the same iris geometry has been experimentally tested at MIT using the MIT/Haimson accelerator [9]. This experiment was conducted with a train of 1 ps bunches spaced at 17 GHz. This was modeled in the PIC module in CST using a multibunch excitation. The simulated PBG structure, shown in Fig. 1, had seven cells to be consistent with the other simulations shown here, and to reduce computation time used uniform cells instead of the coupling cells and waveguides used in [9]. The simulation used an on-axis train of 1 ps long bunches separated by 58.1 ps to simulate the long bunch train of the experiment. The total charge of one bunch is 20 pC, corresponding to 344 mA current. The longitudinal E-fields are calculated on axis.

The longitudinal E-fields at the center of a cell on the beam axis and 35 mm off the beam axis are calculated in CST, showing that most of the energy in the fields is in the fundamental mode, with the second and third harmonics observed approximately 30 dB below the fundamental. The magnitude spectrum of the longitudinal E-field calculated outside the structure about 35 mm away from the beam reveals that the fundamental mode is well confined to the defect area, but the second harmonic, whose frequency is in the passband of the lattice, propagates out of the lattice with a small decrease in amplitude. Three dipole modes can be recognized with much lower energy. Because of the coherence, the fields at the beam train's frequency (17.2 GHz) and its harmonics (34.4 GHz, 51.6 GHz, etc.) are enhanced, so the energy in the dipole modes is much lower than the fundamental modes and the harmonics. The calculated E-field at the fundamental is about 10 dB lower than that at the second harmonic, which agrees well with the experimental results measured outside the chamber window [9].

As a check on the applicability of the simulation results to experiment, we can compare the beam loading in the simulation to the beam loading in the theory and the experiment [9]. From the theory [29], the longitudinal electric field induced by the beam after traversing a distance l should be

$$E_b = ir_s(1 - e^{-Il}), \tag{5}$$

where i is the beam current, r_s is the shunt impedance per unit length, and I is the voltage loss per unit length. I can be described as a function of frequency (ω), group velocity (V_g), and quality factor (Q) of the structure [30]:

$$I = \frac{\omega}{2V_g Q}. \tag{6}$$

From Eqs. (5) and (6), we can calculate the magnitude of the E-field induced by the bunched beam. The theoretical magnitude of E_b in the middle of the sixth cell (i.e. at $z =$ 32.6 mm) is calculated to be 3.4×10^6 V/m, using $V_g = 0.013c$, $r_s = 98$ MΩ/m, $Q = 4200$ [8], and beam current $i = 344$ mA. In the CST simulation the steady-state amplitude of E_b measured on axis in the middle of the fifth cell, when driven by a train of on-axis bunches, is observed to be 4.6×10^6 V/m. This result agrees reasonably well with the theory.

We can calculate the induced power using

$$P_b = \frac{E_b^2}{2Ir_s} = \frac{E_b^2 V_g Q}{\omega r_s} = \left(\frac{i^2 r_s}{2I}\right)(1 - e^{-Il})^2. \tag{7}$$

Substituting Eq. (6) into Eq. (7), we obtain

$$P_b = \left(\frac{i^2 r_s V_g Q}{\omega}\right)\left[1 - \exp\left(-\frac{\omega l}{2V_g Q}\right)\right]^2. \tag{8}$$

Because $\frac{\omega l}{2V_g Q}$ is much smaller than 1, we can use Taylor series expansion to get the following expression:

$$P_b = i^2 \frac{\omega l^2 r_s}{4V_g Q}. \tag{9}$$

Using the steady-state field amplitude from the simulation and Eq. (7), the electromagnetic power induced by the beam in the simulation is calculated to be 33 kW. By comparison the theoretical power induced by the beam after 32.6 mm is 20 kW.

From [9] we can extrapolate the experimental value of the power induced by a 344 mA current beam, giving a value of approximately 13 kW in a six-cell PBG structure with two ports coupling the field at the first and the sixth cells. This coupling makes the effective length of the structure at the measurement location shorter by approximately the length of one full cell, making the effective length 26.7 mm instead of the 32.6 mm used in the simulation. In Eq. (8) we can see that the power induced by the beam scales as the square of the length. If we scale the power predicted by the CST result, we find a beam induced power of 21 kW. This represents reasonable agreement between the power induced by the beam in the simplified geometry used in the simulation and the power induced by the beam that was observed experimentally.

VI. CONCLUSION

The longitudinal and transverse wake potentials excited by an electron beam in a traveling-wave PBG structure have been simulated using CST PARTICLE STUDIO. Simulation of a disk-loaded waveguide structure with the same iris geometry shows that the PBG structure can effectively confine the fundamental mode and damp the dipole modes excited by the bunch. While the results presented here are for seven-cell structures, simulations with six-cell structures have shown excellent agreement.

The wake potential impedances for the longitudinal and transverse wakes were calculated from the time-domain wake potentials using MATLAB. Numerical filters were used to isolate each mode from the wake potential spectrum. This frequency information was then used to recover the contribution to the wake potential from each mode; this provides the $1/e$ decay distance for each mode.

The modes observed in CST simulations of the PBG structure were confirmed using single-cell eigenmode simulations in HFSS. The single-cell simulations were used to confirm the frequency of the observed mode, and then to provide a Q factor for that mode for quantitative comparison. These simulations showed reasonable agreement between the decay distances of the wakes observed in the frequency domain (HFSS) and particle-in-cell (CST) simulations for the fundamental mode and the three lowest-frequency dipolelike modes.

The combination of particle-in-cell (CST) and frequency-domain (HFSS) simulations provides an effective method by which to study the wakefield damping in the latest PBG structures. The testing of these structures, e.g., the elliptical-rod PBG structure tested at SLAC by MIT and described in [27], has focused on achieving the highest gradient possible in a PBG structure. The achieved gradient cannot be easily predicted from simulation, so the use of PIC simulations for wakefield damping allows the experimental efforts to continue to focus on achieved gradient.

The PBG lattice was found to have dipolelike modes with peaks in field amplitude within the lattice, giving rise to three dipole modes which are excited with similar amplitudes over a 4 GHz frequency range in the three-row PBG lattice. CST simulations confirmed that the number of distinct dipole modes in the PBG lattice is determined by the number of rows of rods in the structure. This means that, while going to a larger number of rows gives a larger diffractive Q factor for the fundamental mode, more dipole modes are supported in these larger structures.

A comparison of the transverse wake potentials of the PBG and DLW structures shows that the PBG structure does not significantly alter the initial excitation of HOMs, based on the initial amplitude of the wake potential, but the PBG does damp the wake potential much faster than the DLW structure. This validates the use of the HOM Q as a design metric for future PBG structures.

In addition to the single bunch simulations used to investigate the wake potential in the PBG structure, a bunch train spaced at the fundamental frequency of the structure was also simulated. This reflects the micro-bunched beam used the MIT experiment to study wakefields in the traveling-wave PBG structure. The full experimental geometry could not be simulated, but the beam loading calculated in the CST simulation agrees with the experimental beam loading.

ACKNOWLEDGMENTS

The authors thank Zenghai Li from SLAC and Emilio Nanni and Sergey Arsenyev from PSFC, MIT for helpful discussions. The work is supported by Department of Energy High Energy Physics, under Contract No. DE-FG02-91ER40648 and Fundamental Research funds for the Central Universities under Contract No. ZYGX 2010J055.

[1] B. Aune, R. Bandelmann, D. Bloess, B. Bonin, A. Bosotti, M. Champion, C. Crawford, G. Deppe, B. Dwersteg, D. A. Edwards *et al.*, Phys. Rev. ST Accel. Beams **3**, 092001 (2000).

[2] T. Shintake, Jpn. J. Appl. Phys. **31**, L1567 (1992).

[3] T. Shintake, H. Matsumoto, N. Akasaka, M. Yoshida, C. Adolphsen, K. Jobe, D. McCormick, M. Ross, and T. Slaton, in *Proceedings of the 18th Particle Accelerator Conference, New York, 1999* (IEEE, New York, 1999), Vol. 5, pp. 3411–3413.

[4] Z. Li, N. Folwell, L. Ge, A. Guetz, V. Ivanov, M. Kowalski, L.-Q. Lee, C.-K. Ng, G. Schussman, L. Stingelin *et al.*, Nucl. Instrum. Methods Phys. Res., Sect. A **558**, 168 (2006).

[5] R. M. Jones, C. E. Adolphsen, J. W. Wang, and Z. Li, Phys. Rev. ST Accel. Beams **9**, 102001 (2006).

[6] W. Wuensch, in *Proceedings of the 11th European Particle Accelerator Conference, Genoa, 2008* (EPS-AG, Genoa, Italy, 2008).

[7] D. R. Smith, S. Schultz, N. Kroll, M. Sigalas, K. M. Ho, and C. M. Soukoulis, Appl. Phys. Lett. **65**, 645 (1994).

[8] E. I. Smirnova, A. S. Kesar, I. Mastovsky, M. A. Shapiro, and R. J. Temkin, Phys. Rev. Lett. **95**, 074801 (2005).

[9] R. A. Marsh, M. A. Shapiro, R. J. Temkin, E. I. Smirnova, and J. F. DeFord, Nucl. Instrum. Methods Phys. Res., Sect. A **618**, 16 (2010).

[10] S. Schultz, D. Smith, and N. Kroll, in *Proceedings of the Particle Accelerator Conference, Washington, DC, 1993* (IEEE, New York, 1993), pp. 2559–2563, Vol. 4.

[11] G. R. Werner, C. A. Bauer, and J. R. Cary, Phys. Rev. ST Accel. Beams **12**, 071301 (2009).

[12] M. R. Masullo, A. Andreone, E. Di Gennaro, S. Albanese, F. Francomacaro, M. Panniello, V. G. Vaccaro, and G. Lamura, Microw. Opt. Technol. Lett. **48**, 2486 (2006).

[13] A. M. Cook, B. J. Munroe, M. A. Shapiro, and R. J. Temkin, in *Proceedings of the 2011 Particle Accelerator Conference, NY, USA* (IEEE, New York, 2011), pp. 175–177.

[14] K. L. F. Bane, P. B. Wilson, and T. Weiland, AIP Conf. Proc. **127**, 875 (1985).

[15] P. B. Wilson, AIP Conf. Proc. **184**, 525 (1989).

[16] T. P. Wangler, *Principles of RF linear accelerator* (John Wiley & Sons, Inc., New York, 1998).

[17] B. W. Zotter and S. A. Kheifets, *Impedances and Wakes in High-Energy Particle Accelerators* (World Scientific, Singapore, 1997).

[18] T. Weiland and B. W. Zotter, Part. Accel. **11**, 143 (1981) [http://cds.cern.ch/record/124656].

[19] B. Zotter and K. Bane, Technical Report No. CERN-ISR-TH-80-25. ISR-TH-80-25, 1980.

[20] J. Gao, Nucl. Instrum. Methods Phys. Res., Sect. A **447**, 301 (2000).

[21] G. Dome, IEEE Trans. Nucl. Sci. **32**, 2531 (1985).

[22] E. Keil, Nucl. Instrum. Methods **100**, 419 (1972).

[23] M. A. Shapiro, W. J. Brown, I. Mastovsky, J. R. Sirigiri, and R. J. Temkin, Phys. Rev. ST Accel. Beams **4**, 042001 (2001).

[24] E. Di Gennaro, S. Savo, A. Andreone, V. Galdi, G. Castaldi, V. Pierro, and M. R. Masullo, Appl. Phys. Lett. **93**, 164102 (2008).

[25] C. Jing, F. Gao, S. Antipov, Z. Yusof, M. Conde, J. G. Power, P. Xu, S. Zheng, H. Chen, C. Tang *et al.*, Phys. Rev. ST Accel. Beams **12**, 121302 (2009).

[26] R. A. Marsh, M. A. Shapiro, R. J. Temkin, V. A. Dolgashev, L. L. Laurent, J. R. Lewandowski, A. D.

Yeremian, and S. G. Tantawi, Phys. Rev. ST Accel. Beams **14**, 021301 (2011).

[27] B. J. Munroe, A. M. Cook, M. A. Shapiro, R. J. Temkin, V. A. Dolgashev, L. L. Laurent, J. R. Lewandowski, A. D. Yeremian, S. G. Tantawi, and R. A. Marsh, Phys. Rev. ST Accel. Beams **16**, 012005 (2013).

[28] E. I. Smirnova, Ph.D. thesis, Massachusetts Institute of Technology, 2005.

[29] J. Haimson, Nucl. Instrum. Methods **33**, 93 (1965).

[30] M. Chodorow, E. L. Ginzton, W. W. Hansen, R. L. Kyhl, R. B. Neal, and W. K. H. Panofsky, Rev. Sci. Instrum. **26**, 134 (1955).